Journal of Materials Chemistry C

RSC Publishing

PAPER

View Article Online
View Journal | View Issue

Cite this: *J. Mater. Chem. C*, 2013, **1**, 5149

Received 2nd June 2013
Accepted 20th June 2013

DOI: 10.1039/c3tc31048e

www.rsc.org/MaterialsC

Efficient electroless nickel plating from highly active Ni–B nanoparticles for electric circuit patterns on Al_2O_3 ceramics†

Teng Zhai,[a] Xihong Lu,[a] Guofeng Cui,*[a] Gang Wu,[b] Junxiong Qu[a] and Yexiang Tong[a]

Herein, we report novel and highly-active Ni–B nanoparticles as a precursor for electroless nickel deposition and demonstrate their implementation as high-performance electric circuits on the CCPCB surface.

Introduction

Ceramic cored printed circuit boards (CCPCBs) have attracted great interest recently due to their higher thermal conductivity and reliability relative to traditional organic cored printed circuit boards (OCPCBs). These features make them very promising in high-power light-emitting diodes (LEDs) and electric automobiles.[1] To date, there are two major approaches to fabricate electric circuits on the CCPCB.[2,3] The first one is the thin-filmed circuit process by a physical sputtering method. However, the fabricated electronic conductive metal films are usually too thin to meet the requirements for high current density.[2] The other one is the thick-filmed circuit process by a chemical screen printing method. The conductive film is deposited on the CCPCB surface through a sintered process under high temperature conditions. The thickness of the casted film is hard to accurately control, as the conductive paste is randomly supplied during the sintering.[3] In addition, these two approaches need special instruments or synthetic conditions, which increases the cost. Therefore, the development of a low-cost and efficient method to prepare electric circuits on the CCPCB is highly desirable and may further broaden their applications.

Electroless nickel deposition has emerged as a promising technique that is able to metalize non-conductive materials such as plastics, ceramics and polymers.[4–9] In the metalized process, the catalytic precursor is a key component to catalyze nickel ion reduction spontaneously, which plays an important role in the structure and properties of the as-prepared metal film.[10–12] In most cases, the precursors are usually nickel, cobalt and/or palladium (Pd) particles/sol.[12–14] However, due to the smooth surface of CCPCB, these catalytic precursors could not be strongly adhered on the alumina substrate of the CCPCB. On the other hand, these catalytic species need to be stabilized on the alumina under high temperature conditions.[15] Unfortunately, the relevant literature for exploring effective catalytic species and relevant heating treatment using electroless nickel deposition is insufficient for developing CCPCB technology. Ni–B has been widely studied in electroless nickel deposition owing to its high activity, good selectivity and strong sulfur poison resistance, as well as its environmental friendliness.[16–18] In comparison with precious metal-based catalysts (Pd, Pt, Ag, Au), it has comparable catalytic activity and lower cost.[19,20] Therefore, the development of Ni–B is highly desirable. In this paper, we report novel and highly-active Ni–B nanoparticles as a precursor for electroless nickel deposition and demonstrate their implementation as high-performance electric circuits on the CCPCB surface.

Results and Discussions

The highly-active Ni–B nanoparticle sol was synthesized in ethanediol at 5.0 ± 2.0 °C (experimental section, ESI†). The sol

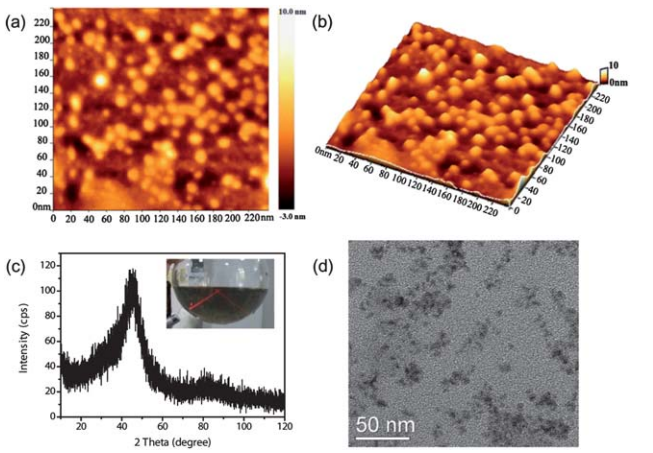

Fig. 1 (a and b) AFM images, (c) XRD pattern and (d) TEM image of the Ni–B nanoparticles. The inset in (c) is an optical image of the Ni–B nanoparticles.

[a]*Key Laboratory of Low-carbon Chemistry & Energy Conservation of Guangdong Province, Huizhou Research Institute of Sun Yat-sen University, School of Chemistry and Chemical Engineering, Sun-Yat Sen University, GuangZhou, 510275, P.R. China. E-mail: cuigf@mail.sysu.edu.cn*

[b]*Materials Physics & Applications Division, Los Alamos National Laboratory, Los Alamos, NM 87545, USA*

† Electronic supplementary information (ESI) available: SEM images, XRD patterns. See DOI: 10.1039/c3tc31048e

is black in color and very stable with no precipitation (inset in Fig. 1c). A typical Tyndall effect could be easily observed in the 0.1 mol L^{-1} Ni–B sol by a red laser beam (inset in Fig. 1c). Atomic force microscopy (AFM) was performed to identify the morphology of the Ni–B sol. Fig. 1a and b show typical AFM images of the Ni–B sol, clearly revealing that the sol consists of a large number of Ni–B nanoparticles. These Ni–B nanoparticles have a uniform diameter of about 10–20 nm. We found that these Ni–B nanoparticles can be easily absorbed into the cavities of roughened alumina substrates in subsequent steps. To determine the phase and crystalline structure of the product, the X-ray diffraction (XRD) pattern collected from the as-prepared sample is shown in Fig. 1c. Only one broad and weak peak was detected in this pattern, suggesting that these Ni–B nanoparticles have a poorly crystalline nature.

To evaluate the catalytic activity of the Ni–B nanoparticles, cyclic voltammetry (CV) plots collected from the pure Ni sheet and Ni–B nanoparticles in different solutions with and without hypophosphite and nickel sulfate at 80 °C are shown in Fig. 2a. No peak can be observed in the absence of hypophosphite and nickel sulfate. On the contrary, obvious anodic peaks located between 0.9 and 1.1 V were observed for both the Ni sheet and Ni nanoparticles when the solution contained hypophosphite and nickel sulfate. The oxidative peaks in CV are associated with the oxidation of hypophosphite ($NiOOH + H_2PO_2^- \rightarrow NiO + H_2PO_3^- + H^+ + e^-$). In nickel electroless deposition, it is necessary for the oxidation reactions to release electrons, providing them for the Ni^{2+} ion reduction reactions. The electrons are provided from a source of hydrogen radicals, which is generated during the breakage of P–H bonds in hypophosphite.[15,21,22] The hydrogen radical can combine with a hydroxyl ion and then release one electron as follows:

$$Ni(OH)_2 + OH^- \rightarrow NiOOH + H_2O + e^-$$

The standard potential of the above reaction is 0.488 V *vs.* SHE at 25 °C.[23,24] According to the Nernst equation, the oxidation peak of NiOOH can be observed at around 0.78 V at pH = 5.5 and 80 °C. Given that the geometrical area of electrodes was the same, the Ni–B nanoparticles exhibited a much higher anodic current and a larger peak area (about 1.9 times larger) than the Ni sheet, confirming the superior electrocatalytic activity of the Ni–B electrode. Zhang *et al.* studied the catalytic activity of Ni–B nanoparticles and crystalline Ni nanoparticles with similar surface area, and they found that the Ni–B nanoparticles exhibited better catalytic activity due to the modification of the electronic properties of Ni by B.[29] Therefore, in our case, the enhanced catalytic activity of the Ni–B nanoparticles is attributed to the larger electrochemically accessible surface area and the modification of the electronic properties.[25,28,30–32]

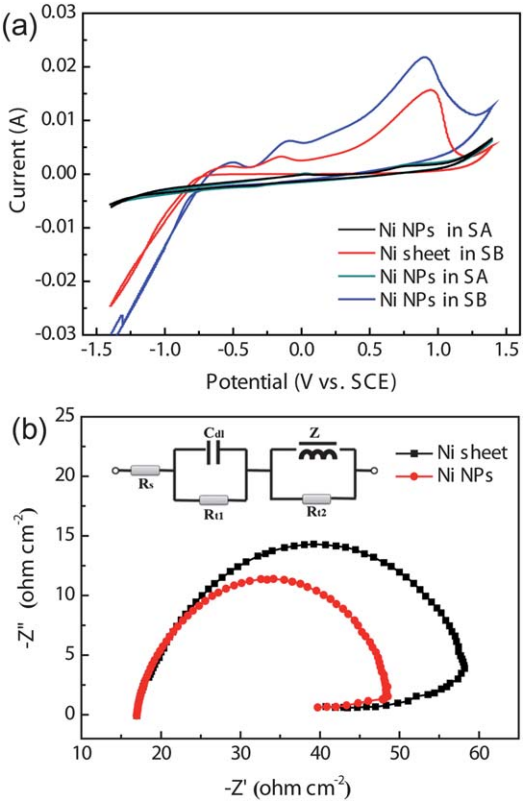

Fig. 2 (a) CV curves of the Ni sheet and Ni–B nanoparticle electrodes in solution with (SB) and without (SA) hypophosphite and nickel sulfate at a temperature of 80 °C and at a scan rate of 10 mV s^{-1}. (b) Nyquist plots of the Ni sheet and Ni–B nanoparticle electrodes in a solution with hypophosphite at a temperature of 80 °C. Inset: equivalent circuit simulating the EIS data.

Electrochemical impedance spectroscopy (EIS) measurements were also performed in the solution containing hypophosphite and nickel sulfate at 80 °C to further investigative the catalytic activity. Fig. 2b shows the Nyquist plots of the Ni sheet and the Ni–B nanoparticles. Two loops were observed for the Ni–B nanoparticles and Ni sheet. The capacitive loop (CL-H) is in the high-frequency domain, while the inductive loop (IL-L) is in the low-frequency domain. To better understand the behavior of these electrodes, an equivalent circuit was used to simulate the EIS spectra (inset in Fig. 2b). Generally, the observed CL-H in electrochemical reactions can be correlated to the charging and discharging process of electrical double layers at the electrode/solution interface. The loop diameter is dependent on the charge-transfer resistance (R_{ct1}). Significantly, the R_{ct1} of the Ni–B nanoparticles is 31.6 Ω cm^{-2}, which is substantially smaller than the value obtained from the Ni sheet (41.6 Ω cm^{-2}). This clearly indicates that the Ni–B nanoparticles exhibit a higher catalytic activity for electroless nickel ion reduction than the Ni sheet.

To test their feasibility for application on CCPCBs, an electronic circuit was fabricated on an alumina ceramic substrate based on these Ni–B nanoparticles. The electric circuit fabrication process on the alumina ceramic substrate is described in Fig. 3a. Firstly, the ceramic surface was roughened to enhance the adhesion between the metallic coating and the ceramic substrate. Additionally, in order to examine the surface characteristics of the alumina substrate during the metalization process, we also studied the morphology and structure using SEM and XRD analyses as a function of the fabrication steps. From Fig. S1,† we can observe that many cavities appeared on the surface of the alumina ceramic substrate after the

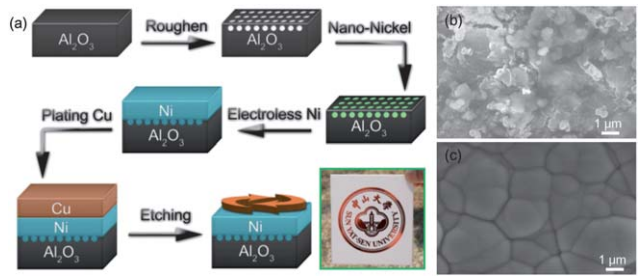

Fig. 3 (a) Electric circuit fabrication process on an alumina ceramic substrate. Inset: optical image of a metallic pattern of our university logo on the alumina ceramic substrate. SEM images of the ceramic substrate surface (b) after the Ni–B nanoparticle coating (after heat treatment at 200 °C for 15 min) and (c) after electroless nickel deposition.

roughening treatment (for details see ESI†). These cavities can act as "parasitic sites" for Ni–B nanoparticles. Then, the Ni–B nanoparticle sol was coated on the treated Al_2O_3 substrate. In order to cure the Ni–B nanoparticle sol, the ceramic substrate coated with Ni–B species was heated at 200 °C for 15 min in air. The SEM image in Fig. 3b reveals a large number of Ni–B nanoparticles permeated into the micro-scaled cavities in the ceramic substrate. Then, to further enhance the connection between Al_2O_3 and the Ni–B film, the ceramic substrate was annealed at 600 °C. The literature has reported that the alloying temperature of Ni–B starts at 300 °C,[33–35] but we found that the connection between Al_2O_3 and the Ni–B film annealed at 600 °C was superior in this case. Subsequently, electroless nickel planting was performed on the activated alumina substrate in a solution containing 25.0 g L^{-1} $NiSO_4 \cdot 6H_2O$, 30.0 g L^{-1} NaH_2PO_2, 12.0 g L^{-1} sodium acetate, 8.0 g L^{-1} lactic acid and 5.0 g L^{-1} citric acid. In this step, Ni–B nanoparticles serve as catalytic active cites for the electroless nickel ion reduction reaction.[26,27] In Fig. 3c, the cavity structure of the ceramic substrates has disappeared. A smooth and uniform ceramic substrate was obtained after covering with a layer of Ni. XRD analysis (Fig. S3†) indicates that the Ni layer is amorphous. More importantly, our present method can be easily used to fabricate various electric circuit patterns. As shown in Fig. 3a, a metallic pattern of our university logo was successfully fabricated on the ceramic substrate. In addition, to meet the demand for high-power light-emitting diodes (LEDs) and electric automobiles, the electric circuit pattern should have a high conductivity. In our case, the conductivity of the ceramic substrates can be readily controlled by simply adjusting the deposition time or by subsequent copper electroplating. As shown in Fig. 4, the conductivity of the ceramic substrates was greatly improved from 0 to 0.97 S cm^{-1} after 10 min of electroless nickel deposition. On the other hand, the electronic conductivity could also be further improved by applying a copper coating, and it can reach 2.3 S cm^{-1} after 5 min of Cu electroplating. Finally, to demonstrate their practical application, we used the as-prepared films on a ceramic substrate to fabricate high-powered LED circuits. On the copper circuits' surface, ten 10 W LED chips were packaged onto the 50 × 80 mm^2 area. The LED lamps can steadily illuminate, with no traditional fans to radiate heat.

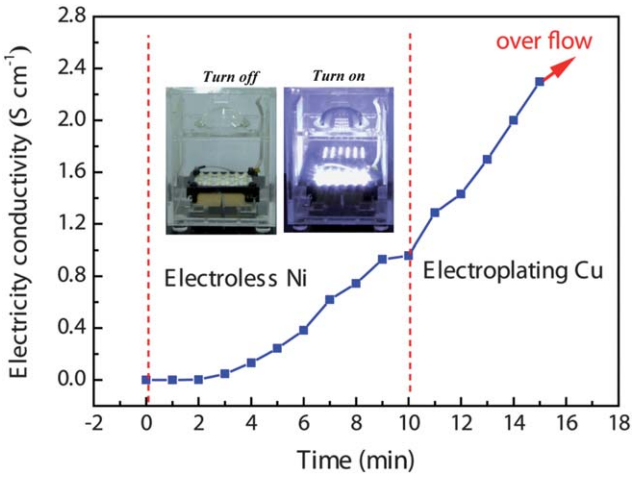

Fig. 4 Electronic conductivity changes of the alumina surface during the electric circuit fabrication process. The initial substrate is alumina coated by the Ni–B nanoparticle sol after heat treatment at 200 °C for 15 min. Inset: optical image showing a 100 W high-powered LED lamp.

Conclusions

In summary, stable and highly-active Ni–B nanoparticles have been prepared for electroless nickel deposition. These Ni–B nanoparticles, with a diameter of 10–20 nm, exhibit a higher catalytic activity than the traditional Ni sheet in the electroless nickel deposition reaction. In addition, the conductivity of the electric circuit on an alumina ceramic substrate can be readily tuned by adjusting the Ni and Cu deposition times. More importantly, the electric circuit on the CCPCB surface prepared by using these Ni–B nanoparticles as catalytic active sites has excellent performance in high-powered LEDs.

Acknowledgements

Dr G. F. Cui gratefully acknowledges the financial support by the National Natural Science Foundation of China (51271205), "the Fundamental Research Funds for the Central Universities" (11lgpy08), "Guangzhou Pearl Technology the Nova Special Project" (2012J2200058), "Research and Application of Key Technologies Oriented the Industrial Development" (90035-3283309), "Plan of Science and Technology Project" by the DaYa Gulf district in Huizhou city (31000-4207387), and the Innovative Laboratory Fund by Sun Yat-Sen University.

Notes and references

1 T. Jeong, K. H. Kim, S. J. Lee, S. H. Lee, S. R. Jeon, S. H. Lim, J. H. Baek and J. K. Lee, *IEEE Photonics Technol. Lett.*, 2009, **21**, 890–892.
2 G. E. Ponchak, E. Dalton, M. M. Tentzeris and J. Papapolymerou, *IEEE Trans. Adv. Packag.*, 2005, **28**, 320–327.
3 K. Kordas, A. E. Pap, J. Saavalainen, H. Jantunen, P. Moilanen, E. Haapaniemi and S. Leppavuori, *IEEE Trans. Adv. Packag.*, 2005, **28**, 259–263.
4 I. Lee, P. T. Hammond and M. F. Rubner, *Chem. Mater.*, 2003, **15**, 4583–4589.

5 H. Ogihara, A. Hara, K. Miyamoto, N. K. Shrestha, T. Kaneda, S. Ito and T. Saji, *Chem. Commun.*, 2010, **46**, 442–444.
6 A. M. Bazargan, S. Ghashghai, M. Keyanpour-rad and M. E. Ganji, *RSC Adv.*, 2012, **2**, 1842–1845.
7 W. S. Choi, H. R. Jung, S. H. Kwon, J. W. Lee, M. L. Liu and H. C. Shin, *J. Mater. Chem.*, 2012, **22**, 1028–1032.
8 Z. Liu, Z. Li, F. Wang, J. Liu, J. Ji, K. C. Park and M. Endo, *Mater. Res. Bull.*, 2012, **47**, 338–343.
9 X. Chen, W. Yang, S. Wang, M. Qiao, S. Yan, K. Fana and H. He, *New J. Chem.*, 2005, **29**, 266–268.
10 G. F. Cui, N. Li, D. Y. Li and M. L. Chi, *J. Electrochem. Soc.*, 2005, **152**, C669–C674.
11 H. Ogihara, T. Katayama and T. Saji, *J. Mater. Chem.*, 2011, **21**, 14890–14896.
12 S. Y. Cheon, S. Y. Park, Y. M. Rhym, D. H. Kim and J. H. Lee, *Curr. Appl. Phys.*, 2011, **11**, 790–793.
13 Z. J. Wu, M. H. Zhang, S. H. Ge, Z. L. Zhang, W. Li and K. Y. Tao, *J. Mater. Chem.*, 2005, **15**, 4928–4933.
14 Z. G. An, J. J. Zhang and S. L. Pan, *Dalton Trans.*, 2010, **39**, 3378–3383.
15 T. Homma, A. Tamaki, H. Nakai and T. Osaka, *J. Electroanal. Chem.*, 2003, **559**, 131–136.
16 T. S. N. S. Narayanan and S. K. Seshadri, *J. Alloys Compd.*, 2004, **365**, 197–205.
17 T. S. N. S. Narayanan, K. Krishnaveni and S. K. Seshadri, *Mater. Chem. Phys.*, 2003, **82**, 771–779.
18 W. Wang, B. Gu, L. Liang and W. A. Hamilton, *J. Phys. Chem. B*, 2004, **108**, 17477–17483.
19 J. Geng, D. A. Jefferson and B. F. G. Johnson, *Chem.–Eur. J.*, 2009, **15**, 1134–1143.
20 S. B. Kalidindi, A. A. Vernekar and B. R. Jagirdar, *Phys. Chem. Chem. Phys.*, 2009, **11**, 770–775.
21 T. Homma, I. Komatsu, A. Tamaki, H. Nakai and T. Osaka, *Electrochim. Acta*, 2001, **47**, 47–53.
22 H. Nakai, T. Homma, I. Komatsu and T. Osaka, *J. Phys. Chem. B*, 2001, **105**, 1701–1704.
23 W. G. Tam and J. S. Wainright, *J. Power Sources*, 2007, **165**, 481–488.
24 G. M. Wang, X. H. Lu, T. Zhai, Y. C. Ling, H. Y. Wang, Y. X. Tong and Y. Li, *Nanoscale*, 2012, **4**, 3123–3127.
25 G. F. Cui, H. Liu, G. Wu, J. W. Zhao, S. Q. Song and P. K. Shen, *J. Phys. Chem. C*, 2008, **112**, 4601–4607.
26 F. Erler, C. Jakob, H. Romanus, L. Spiess, B. Wielage, T. Lampke and S. Steinhauser, *Electrochim. Acta*, 2003, **48**, 3063–3070.
27 C. N. R. Rao, G. U. Kulkarni, P. J. Thomas and P. P. Edwards, *Chem. Soc. Rev.*, 2000, **29**, 27–35.
28 Z. Wu, J. Zhao, M. Zhang, W. Li and K. Tao, *Catal. Commun.*, 2010, **11**, 973–976.
29 Z. Wu, J. Chen, Q. Di and M. Zhang, *Catal. Commun.*, 2012, **18**, 55–59.
30 S. Ge, Z. Wu, M. Zhang, W. Li and K. Tao, *Ind. Eng. Chem. Res.*, 2006, **45**, 2229–2234.
31 Z. Wu, M. Zhang, S. Ge, Z. Zhang, W. Li and K. Tao, *J. Mater. Chem.*, 2005, **15**, 4928–4933.
32 Z.-J. Wu, S.-H. Ge, M.-H. Zhang, W. Li, S.-C. Mu and K.-Y. Tao, *J. Phys. Chem. C*, 2007, **111**, 8587–8593.
33 S. Wei, Z. Li, S. Yin, X. Zhang, W. Liu and X. Wang, *J. Synchrotron Radiat.*, 2001, **8**, 566–568.
34 Z. Jiang, H. W. Yang, Z. Wei, Z. Xie, W. J. Zhong and S. Q. Wei, *Appl. Catal., A*, 2005, **279**, 165–171.
35 S. Q. Wei, H. Oyanagi, Z. R. Li, X. Y. Zhang, W. H. Liu, S. L. Yin and X. G. Wang, *Phys. Rev. B: Condens. Matter*, 2001, **63**, 224201–224206.

